Pressure Fluctuations on the Open Ocean Floor Over a Broad Frequency Range: New Program and Early Results

J. H. FILLOUX

Scripps Institution of Oceanography, La Jolla, CA 92093

(Manuscript received 2 June 1980, in final form 15 August 1980)

ABSTRACT

A two-month ocean-floor pressure record obtained 330 km to the east of the main island of Hawaii by means of a Bourdon tube-type transducer with optical readout is discussed in detail. An approach to subtraction of the drift component associated with plastic flow of the heavily strained transducer is assessed. In spite of a 40 m progressively accumulated error, it is shown that fluctuations with periods as long as a few cycles per record length are resolved with a remarkable precision. The lunar fortnightly tide, with its period around 14 days, for instance, appears to be in error by no more than 0.3 cm, on the assumption that the transfer function between gravitational driving corrected for earth tides and sea floor pressure has a modulus of 0.7 and a negligible phase shift.

Eleven tidal constituents in each of the diurnal and semidiurnal bands, as well as constituents M3 and Mf are tabulated. These estimated tidal constants come within a few percent of those published for Hilo, revealing a relative uniformity of tidal behavior for this area. The use of tide constants from Hilo to check or to constrain mathematical models of the Pacific tides thus appears acceptable.

Because of its inherent high-frequency response and its high accuracy (response up to 1 cycle per second; resolution 0.0206 cm in present data) the instrumentation used in the experiment described here can contribute to the investigation of a variety of problems of ocean geophysics. For instance, the low-frequency end of the surface wind-generated wave spectrum is clearly resolved and is shown to vary slowly from day to day with considerable variations over weekly or longer time spans.

The close approach on 20 July 1978 of Tropical Cyclone Fico to the area of our sea-floor station provided an opportunity to investigate its effect on sea-floor pressure fluctuations. Although somewhat disappointing, this attempt does stress the great advantage to be gained by using an array of stations rather than individual ones to identify and to sort out the many processes at play.

1. Introduction

The behavior of ocean tides away from coast lines and islands is still so poorly understood that a program solely dedicated to their observation is justifiable (Zetler, 1967; Munk and Zetler, 1967; Cartwright *et al.*, 1979).

Although not exactly easy to perform, pressure measurements on the sea floor constitute at present the most effective approach to estimate tidal fluctuations of sea level over the open ocean (Caldwell *et al.*, 1969; Filloux, 1969, 1970, 1973, 1979; Munk *et al.*, 1970). The information contained in these sea-bottom pressure recordings, however, may contribute to the investigation of an extended range of phenomena of ocean geophysics besides that of tides alone.

With a resolution of 0.02 cm or less, a sampling rate possibly as fast as 2 per second (for 50 hours), an endurance extendable to a year or more (at 32 samples per hour), and drift characteristics sufficiently well understood to negate to a large extent the damaging effects of this hardly avoidable limitation, the instrumentation referred to in this paper can also be useful for the study of storm-induced high-frequency pressure noise in the ocean (Latham *et al.*, 1967); of microseisms generation (Longuet-Higgins, 1950; Hasselmann, 1963) and propagation (Oliver and Dorman, 1961; Haubrich *et al.*, 1963); of the very low-frequency end of the wind-wave spectrum (Munk, 1947a), in particular its yet unobserved very low-frequency end ($T > 1$ min; Snodgrass *et al.*, 1966); perhaps of certain aspects of internal waves and internal tides (Garrett and Munk, 1975); of tsunamis (Munk, 1962); of certain modes of planetary waves (Wunsch and Gill, 1976) of very long-period and very large-scale dynamic features of oceanic circulation (Wyrtki, 1974, 1975), and perhaps also of certain interactions between ocean and atmosphere associated with extended winter storms at moderate and high latitudes (Philander, 1978; Frankignoul and Müller, 1979).

The data discussed here result from the initial test of a modernized version of an earlier Bourdon-tube-type pressure sensor (Filloux, 1969). The location of the station, 18°56'N, 152°29'W (i.e., about 330 km east of Hilo, Hawaii) was fortuitous: the

0022-3670/80/121959-13$07.25

experiment was performed simultaneously with other operations in deep water associated with electromagnetic investigations of the oceanic mantle (Filloux, 1980, 1981).

One objective of this paper is to illustrate the possibilities listed above. With a single instrument at a single site the information available is extremely restricted. In particular, propagation properties of recorded features cannot be studied, thereby limiting considerably our ability to identify their nature and origin. Nevertheless, considerations such as sensitivity, stability, frequency response, and the establishing of limits on signal-to-noise ratios over a vast frequency range on the deep-sea floor convey a very favorable image of the potential usefulness of pressure observations carried out on the bottom of the open ocean.

2. Instrumentation

With the availability today of large-volume and reliable data-logging equipment the quality of pressure recording on the open oceanic sea floor strictly depends upon the transducers. Of these, the most often used include vibrating string devices such as vibrotrons (Eyriés *et al.*, 1964; Nowroozi *et al.*, 1966; Snodgrass, 1968), strain gage devices (Hicks *et al.*, 1965; Wunsch and Dahlen, 1974), specially shaped quartz crystals (Irish and Snodgrass, 1972; UNESCO, 1975), Bourdon tube, with optical readout (Baker and Wearn, 1973; Filloux, 1969, 1970, 1971), and bellow sensors with quartz crystals as deformation-to-frequency converters (Hayes, 1979). All of these devices suffer from at least one basic deficiency such as temperature dependency, limited sensitivity, restricted frequency response, long-term instability or excessive power requirements. The merits of various sea-floor transducers are discussed in different papers (Munk and Zetler, 1967; Filloux, 1969), and the results of an important intercalibration experiment (UNESCO, 1975) provide a realistic assessment of the performances of several integrated instrument packages.

The transducer used in the sea-floor recorder that collected the data presently discussed is of the multiturn Bourdon-tube type with electrooptical feedback. The sensitivity of this system depends upon a high-resolution angular detector first used in a three-component sea-floor magnetometer (Filloux, 1980). The simultaneous achievement of large dynamic range and exceptional sensitivity results from an opto-electronic design with a sixteen-bit long-term accuracy associated with a recording scheme that registers only occasionally the most significant eight-bit byte. This scheme constitutes a considerable simplification over an earlier one (Filloux, 1969, 1970) in which an analog equivalent of the present digital overflow accounting depended on the perfection of a multinull reference achieved by means of very fine-mesh gratings.

The most elusive quality of an open-ocean sea-floor pressure transducer is without doubt its long-term stability. To approach absolute accuracy in a sense useful to oceanographic research, the pressure uncertainty after one year of operation at the average oceanic depth (~5 km) should certainly not exceed 10 cm equivalent water head. No available transducer satisfies this condition.

We have shown in an earlier paper (Filloux, 1969) that the association of a multiturn Bourdon tube made of an optimum, properly heat-treated ferro-nickel alloy (Ni Span C) with a frictionless electro-optical readout device can lead to a pressure transducer principle in which the drift due to plastic flow, although quite large, is sufficiently well defined and understood to be largely compensable for. The present data confirm this earlier conclusion. The subtraction from the raw data of a simple, analytically generated, monotonic and inherently smooth function of time very close to Andrade's Beta creep law (Andrade, 1910; Mott, 1953) results in a time series where readily visible long-term features of very small amplitude could in no way be generated by the drift correction scheme.

We have also shown in the same paper that this type of pressure sensor is relatively insensitive to temperature as well as to temperature transients and that it can be operated with extremely low power. Another feature of great importance is its inherently fast response.

The other instrumental features necessary to insure high performance do not lead to great complexity. Keeping track of time is now readily achievable through an appropriate utilization of the technology developed by the watch industry. Accordingly, in our instruments the monthly error of the internal quartz clock does not exceed 8×10^{-7} Hz (or 2 s). Additional correction for clock rate could reduce the error further if it were necessary. (For instance, this would be desirable if the time of occurrence of a very well-defined event such as an earthquake had to be accurately identified in the record). Pressure-signal calibration is frozen within quantities inherently unchangeable such as focal length of a lens, elastic constant of Bourdon tube, magnetic moment of a small magnet, or number of turns of a coil. Recording is on Philipps cassettes, with a capacity of 4.2×10^6 bits equivalent to 4×10^5 data points per cassette. The sampling rate is 2^n per hour, n selectable. Thus the endurance or maximum uninterrupted duration of observation is over 4 months at 128 data per hour or 2 months at 256 per hour, etc. The least-count pressure equivalent is also to some extent adjustable through binary division of the voltage controlled oscillator frequency. At 128 data per hour the least count

equivalent is as low as 0.02 cm water head. This is not the ultimate limit by any means.

Since the range of pressure over which the electro-optical feedback operates is much less than the pressure change between surface and bottom, an electromechanical centering system is activated at launching time. This device keeps the light beam properly aligned during the instrument descent to the sea floor. It is then turned off automatically at a preset time.

3. Plastic flow removal

The first step in the data processing consists of recovering the exact value of each data point by adding to the recorded least-significant eight-bit component the appropriate number of overflows or underflows. Occasional recording of the most significant byte insures that no error can result from this data compression. By using the hour rather than the second for time unit and a simple binary subdivision to obtain an appropriate sampling interval, the data collected are automatically synchronous with most standard synoptic observations, providing the instrument clock is reset exactly on the hour (or a binary fraction of the hour). Another necessity is to verify that the clock-rate error remained negligibly small by retiming the instrument clock at recovery.

The unprocessed time series of raw data is plotted on Fig. 1, upper trace. Because of the large plastic flow in the transducer due to abyssal pressure, the tidal fluctuations appear only as tiny ripples. After 57 days of operation the creep has accumulated to an equivalent of 40 m. Although dramatic, this error is in no way as disastrous as it may first appear. This is so for two reasons: 1) much is understood and predictable about the creep pattern, and a high degree of correction is possible, and 2) the transducer can be optimized beyond the present state because several determinant and adjustable parameters are involved (geometry, cold work level, age hardening, thermal shock stabilization).

In the early 1900's, Andrade (1910) observed that plastic flow in heavily cold-worked polycrystalline alloys accumulates at a level proportional to the time under stress to the one-third power. Such Andrade "Beta creep" has often been observed but a plausible mechanism was only recently proposed (Mott, 1953). Although not universal, this functional time dependence of plastic flow is consistent with a fundamental aspect of creep. Namely, at constant stress, creep is smooth, monotonic and it gradually decreases with time. (There is no reason to suppose, contrary to the widespread belief in the existence of a yield point at a sufficiently low stress, that plastic flow can be reduced to zero.

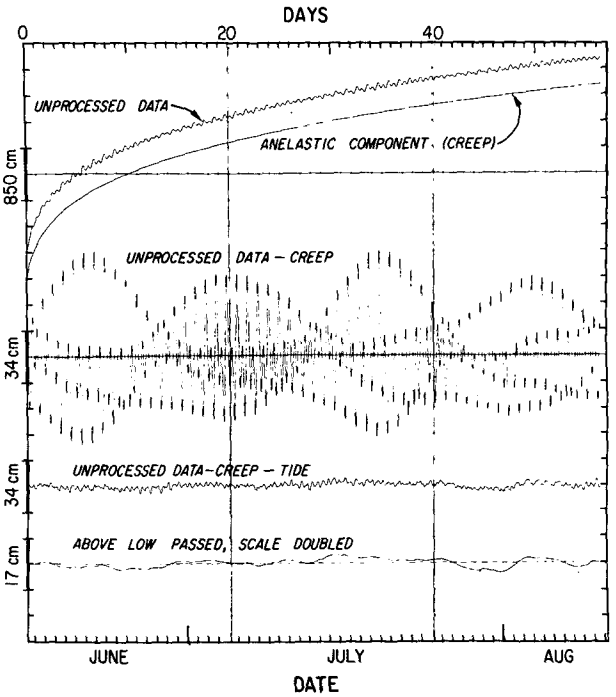

FIG. 1. Traces (from the top): of 1) the raw or unprocessed data; 2) the optimized function representing the plastic flow (or anelastic component) superimposed upon the data as a result of creep; the raw data minus creep (expected to constitute closely the record that a perfect transducer would have obtained); 3) the raw data minus creep and minus the fluctuations coherent with the gravitational tide-driving forces (residual signal); and 4) the residual fluctuations smoothed by means of a 24 h running-average filter. For each curve an appropriate scale is indicated at the left.

In fact, laboratory experiments conducted by means of increasingly sensitive techniques have detected creep at correspondingly reduced thresholds, a result in agreement with our understanding of creep in terms of a stress-assisted, thermally activated process).

There are numerous other analytic functions characterized by the aforementioned properties (e.g., logarithmic or exponential) and, indeed, metallurgic literature speaks of logarithmic as well as of exponential creep. In our experiments neither of these two types of functions of the time T were found to represent the plastic flow of our transducers as well as a power law T^D, although in most instances the value of D was less than the one-third value proposed by Andrade.

In estimating the plastic flow contribution to the data we assume therefore that it is of the form

$$A + B \times (T + C)^D, \qquad (1)$$

where A, B, C and D are constants, T is the time referred to initiation of data recording with A adjusting the datum, B scaling the time dependence,

TABLE 1. Optimum value of drift parameters (units: cm and hour).

A	−742.31
B	871.42
C	6.238
D	0.22698
E_1	−70.60
F_1	6.89
E_2	23.30
F_2	25.75

and C representing the time elapsed between pressurization and start of data logging. The necessity to keep C as a free parameter results from the fact that pressurization is not instantaneous and occurs progressively over the roughly 2 h period during which the instrument falls to the bottom. Furthermore, the touchdown can only be specified to ±0.5 h due to uncertainty in the free fallspeed. Thus C must be very close to the time interval between the instant of touchdown and the preset time at which the automatic centering device maintaining the optical readout alignment during descent is disabled. In the present case the estimated time of arrival on the bottom leads to an initial value $C = 6$ h, later refined to $C = 6.238$ h (see Table 1).

When the optimum values A, B, C, D have been obtained, it is generally found that a small transient remains at the beginning that disappears within a few days. In this case its shape was visibly constituted by two exponential decays with opposite signs and with different time constants. The total drift due to plastic flow was then assumed to be more closely represented by

$$A + B \times (T + C)^D + \sum_1^2 E_i \exp[-(T + C)/F_i], \quad (2)$$

where E_i are the amplitudes and F_i the time constants of the exponential transients. Reoptimization of all free parameters resulted in only minor changes on A, B, C, D. The optimum values of these parameters are listed in Table 1.

The first exponential transient is most probably the expression of the temperature dependence of the instrument in which temperature equalization is slowed down by the large thermal capacity of the battery package. The second is not explained at this time. In any case, if subtraction of these terms is thought to be objectionable, their effects can be eliminated by sacrificing the first four days of data. Since one of our objectives is to show that the consequences of plastic flow can be handled, our case is more convincing if correction of the initial active-creep episode is not avoided artificially by clipping the beginning of the record. Accordingly, all the following data presented start at the time the instrument began recording. It had been on the bottom for approximately 6 h as seen earlier. Pressure and plastic-flow information are not available for this short time span.

The resulting drift function is represented by the second curve from the top of Fig. 1. It includes all terms of Eq. (2). Subtracting it from the raw data (first curve on top of Fig. 1) yields the drift-corrected data, whose quality equals and possibly exceeds that attained by other existing devices [see intercomparison, UNESCO (1975)]. These de-drifted data are plotted at an enlarged scale on Fig. 1, third curve from the top.

4. Subjective assessment of the data

The curve raw-data-minus-creep of Fig. 1 is conspicuously dominated by tides. When the gravitational tide constituents are subtracted (see discussion and results of the tidal analysis in another section) the residual pressure fluctuations are reduced considerably, as apparent on the next curve below. Nevertheless, tidelike ripples remain visible most of the time and fluctuations of very low amplitudes and periods of many days become detectable. These long-term fluctuations are more readily visible on the lower curve of Fig. 1 in which the resolution has been doubled and the data filtered with a simple 24 h running-average low-pass filter.

While a subjective assessment of the usefulness of the present sea-floor pressure record is possible in the case of tides and long-term fluctuations from the considerations above, the existence of valuable high-frequency information seems to disappear completely. In order to show that such useful information is indeed included in the recorded signal, the residual pressure fluctuations following tide removal are plotted with successive resolution-increases by factors of 10, 20 and 5 in Figs. 2, 3 and 4, respectively.

The entire series of residual fluctuations is illustrated in weekly segments in Fig. 2. While diurnal and semidiurnal components are still noticeable, it is obvious that shorter period signals of great variety are present. At the limit of high-frequency resolution the energy in these ripples is seen to be quite variable with time. Three small sections (a–c) characterized by high-, medium- and low-amplitude high-frequency noise, are expanded on Fig. 3.

At this new resolution all individual wave forms at all frequencies appear resolved. All three traces are characterized by episodes of enhanced activity, followed by decreasing and then resumed activity with some form of regularity. This behavior is more visible in the central trace b, and perhaps even more so in the low-signal trace c. We will show that these fluctuations are well above instrumental noise.

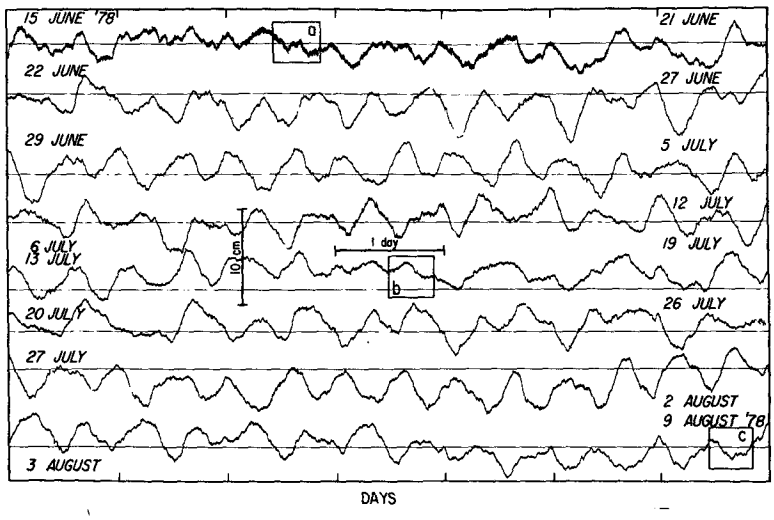

FIG. 2. The residual fluctuations of Fig. 1 plotted with an improved resolution, in weekly segments. Although nearly semidiurnal periodicities are obvious, fluctuations with other, particularly shorter periods are also present. At the highest frequency resolvable, the regime of ripple noise is seen to be quite variable with time.

Again, representative portions of each one of these three pressure fluctuation plots (d–f) are shown at higher resolution in Fig. 4 so as to make individual data points visible. The mean amplitude of the high-frequency fluctuations (>10 cph) is 0.4, 0.2 and 0.1 cm, respectively, for the three traces starting at the top. The individual waves appear so sharply resolved in the absence of any filtering (little superimposed higher frequency noise) that their spectra must steeply decrease before the high-frequency cutoff. At 128 samples per hour, the Nyquist frequency of 64 cph corresponds to a period of 0.94 min. A careful visual search reveals a relative scarcity of features shorter than 2 min. Within the calm intervals separating active areas, including typically 5–10 clear cycles, extremely smooth alignments of data points suggest a very low instrumental noise level (pressure-least-count 0.0206 cm). This subjective observation is strengthened by certain spectral features (see below). The

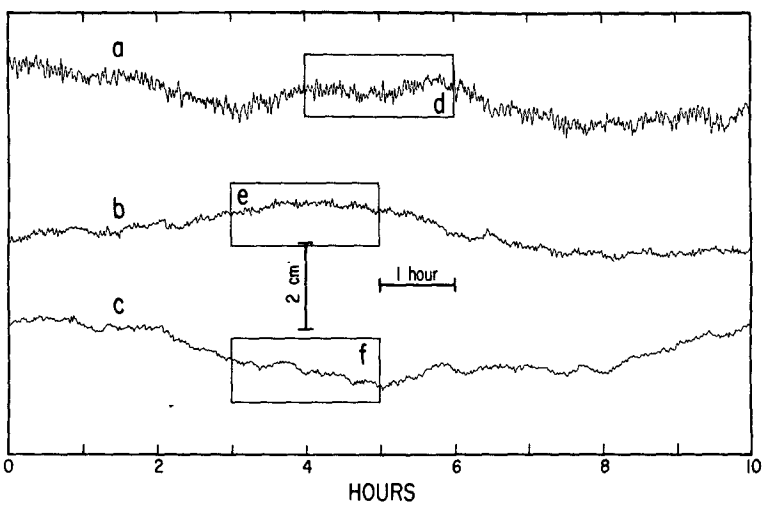

FIG. 3. Three segments (a, b, c) of Fig. 2 characterized by high, medium and low ripple noise are plotted at an increased resolution. All individual waves appear resolved. Particularly visible on the lower trace are successive episodes of high, then low, activity very reminiscent of the beat of waves observed along the coast. These high-frequency fluctuations are probably the signature on the sea floor of the wind-generated surface waves with longest period.

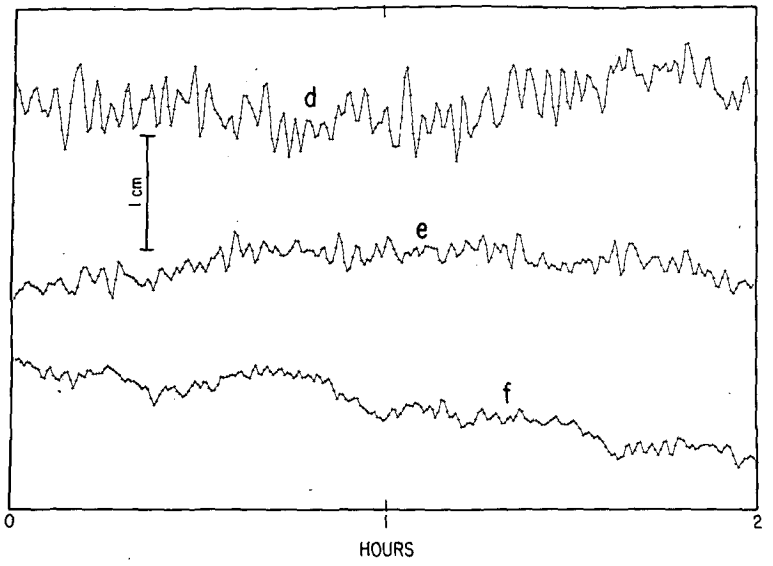

FIG. 4. Three segments (d, e, f) of the traces of Fig. 3 plotted with a resolution sufficiently high to make constitutive data points clearly visible. The mean amplitudes of fluctuations in the band above 6 cph, starting from the top, are 0.4, 0.2 and 0.1 cm. Separation between points: $1/128$ h; least count equivalent water head 0.0206 cm.

close similarity between the observed amplitude modulation and the wave beat noticeable along seashores, as well as the steep high-frequency cutoff at a frequency compatible with the local oceanic depth indicate that the high-frequency pressure fluctuations on Figs. 2, 3 and 4, most likely constitutes the residual signature on the sea floor of the local surface waves. We will return to this subject later.

5. Tides

The familiar tidal pattern with its lunar monthly and semi-monthly beats is clearly visible in the unprocessed data minus creep of Fig. 1. In fact, with 57 days of data, two and four such cycles are almost exactly covered.

The pressure time series has been analyzed in terms of the diurnal and semidiurnal transfer functions—tidal admittances—between gravitational driving and pressure response. The technique used is briefly described in an earlier paper (Filloux, 1971). It involves estimating the successive terms of a Taylor expansion of the admittances as a function of frequency. The optimization procedure consists in minimizing the residual variance between observations and predicted tide. In the present case, on account of the shortness of the record, the expansion was limited to the constant-plus-linear contributions. In both diurnal and semidiurnal bands, the eleven most significant tidal constituents were used, with account taken of the appropriate corrections for nodal variations, which is equivalent to including the principal constituents associated with the 19-year splitting.

The lunar fortnightly and terdiurnal constituents were also included, but no meteorologically driven constituents have been considered. One reason for this omission of radiational contributions is that their effects, significant in the vicinity of land, decrease away from coastal boundaries, although their actual level far offshore is still not well known. Furthermore, since daily meteorological driving can be very randomly modulated, its representation in terms of pure solar and solar harmonic lines constitutes a very coarse approximation.

The estimated constituent amplitudes and phases referred to equilibrium tide at Greenwich are listed in Table 2. These values are compared in Table 3 to the tide constants at the closest Hawaiian permanent tide station of Hilo and with the predictions of Larsen (1977) based on a study of the diffraction of North Pacific tides by the Hawaiian Island chain. The differences are small in both cases, a result principally due to the proximity of the seafloor station to Hilo (separation distance 330 km). Consequently, one can infer not only the correct functioning of the pressure sensor but also the probable adequacy of using Hilo tide data for the purpose of testing and possibly of constraining mathematical modeling of the Pacific Ocean tides over this oceanic area (Hendershott, 1973; Schwiderski, 1980). The tidal fluctuations synthesized from the estimated constituents were then subtracted

TABLE 2. Amplitude and phase of constituents represented in the analysis. Phase is lag behind equilibrium tide at Greenwich except for M3 and Mf where phase is lag at start of record.

Constituent identification	Amplitude (cm)	Phase (deg)
Q1	1.42	−154.5
O1	8.23	−146.2
M1	0.57	−139.3
π1	0.34	−135.0
P1	5.82	−134.7
S1	0.14	−134.3
K1	15.75	−133.9
ψ1	0.14	−133.5
ϕ1	0.26	−133.2
J1	0.91	−129.5
OO1	0.33	−125.9
2N2	0.76	27.1
μ2	0.91	27.4
N2	5.27	29.8
ν2	0.99	30.1
M2	25.00	32.9
λ2	0.17	36.2
L2	0.72	36.8
T2	0.55	40.5
S2	9.23	40.9
R2	0.08	41.3
K2	1.85	41.7
M3	0.2	
Mf	0.84	−15.0

TABLE 3. Comparison of tide constants for sea-floor station (SFS), for Hilo (HL), and for Larsen's predictions (LS).

	Amplitude			Phase		
	SFS	HL	LS	SFS	HL	LS
K1	15.75	16.02	17.0	226.1	234.0	231.0
O1	8.23	8.52	10.0	213.8	223.0	215.0
P1	5.82	4.85	5.5	225.3	232.0	228.0
Q1	1.42	1.51	2.0	205.5	221.0	210.0
M2	20.00	22.3	20.0	32.9	32.0	30.0
S2	9.23	9.0	8.0	40.9	34.0	27.0
N2	5.27	4.5	3.5	29.8	25.0	20.0
K2	1.85	2.4	2.0	41.7	23.0	24.0

from the recorded signal minus the plastic-flow contribution of the transducer. In the following they are referred to as residual fluctuations.

6. Residual pressure fluctuations

The residual pressure fluctuations in the near-tidal and in the inter-tidal bands are best described by the Fourier spectrum (Fig. 5) of the detided data. Beside the rising amplitude trend toward the very low frequencies, three broad peaks are noticeable, centered around the diurnal, semidiurnal and terdiurnal solar and lunar frequencies. These spectral bumps must include the contribution from meteorologically driven fluctuations which, in spite of strong daily modulations, cannot appear as narrow lines since they do not repeat in a perfectly reproducible manner from day to day. They may also result in part from internal tides as discussed by Radok *et al.* (1967). They probably also include a component resulting from the slowly changing overall response of the ocean associated with changes in density structures. Such a possibility appears quite reasonable if oceanic tides are principally representing the relatively high-Q response to those oscillatory modes closely tuned to gravitational excitation. In such a case only small changes in the response are required to produce the observed effect. These spectral bumps must also contain a contribution from the imprecise representation of the gravitational driving mechanism that results from neglecting the smaller constituents. However, this contribution is much too small to explain the cusps [see the extensive list of constituents by Neumann and Pierson (1966)], and in particular it falls off much more rapidly than observed away from the center of the tidal bands. A discussion concerning the origin of tidal cusps around diurnal and semidiurnal tidal bands is given by Munk and Cartwright (1966).

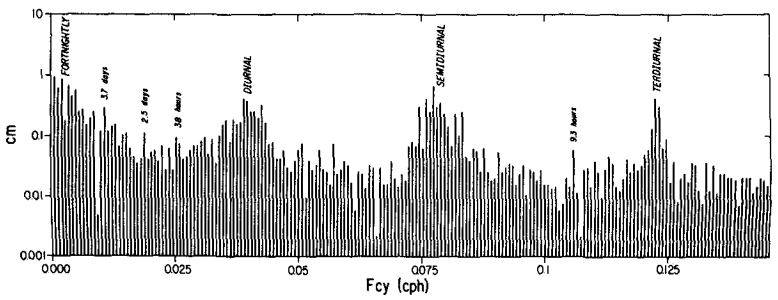

FIG. 5. First 200 lines of the Fourier spectrum of the residual fluctuations when creep and computed tide (Table 2) are subtracted from the raw data (i.e., the time series shown on the second trace from the bottom in Fig. 1 and also in Fig. 2). Note the tidal cusps centered around diurnal, semidiurnal and terdiurnal frequencies. The periods in days of various prominent lines are indicated.

The ambiguity of interpretation of these persistent features emerges from their considerations.

The complete spectrum of the residual pressure fluctuations from the coarsely resolved lower frequency of 0.005 cph up to the Nyquist cut-off at 64 cph is illustrated on Fig. 6. The tidal cusps discussed earlier are also obvious here, accompanied by several daily solar harmonics.

Another distinctive feature in the spectrum of Fig. 6 is the conspicuous bump at the high frequency end. It is smoothly rounded at the top and it ends by a very abrupt dive to the right, suddenly interrupted by a sharp slope reduction. This rapid high-frequency cutoff is implied in the plots of Figs. 3 and 4 in which fluctuations with periods shorter than 2 min are absent. The similarity between the modulation of the high-frequency fluctuations and the beat character of wind waves along sea shores is striking. These arguments suggest that the high-frequency bump results from pressure fluctuations associated with ordinary surface waves with wave lengths and periods long enough to penetrate to the deep-sea floor. This explanation is given considerable support by the specific shape of the estimated subsurface pressure spectrum obtained by dividing the spectrum of sea-floor pressure fluctuations by the relative response on the sea floor of ordinary barotropic surface waves (see Fig. 6). The sea-floor-pressure spectral bump above 10 cph is consistent with the interplay of energy transfer from a process having a natural cutoff slope toward low frequencies—such as regular wind-generated surface waves in the frequency band involved here—through a filter with a response dropping increasingly rapidly in the opposite direction (toward high frequencies). Thus the wave beat observed on the sea floor probably consists of the interaction of surface waves of nearly the same frequencies within the most energetic band of residual sea-floor pressure, just as the wave beat observable along sea shores involves interaction of the most energetic wave components in the local wind-wave regime.

Very low-frequency surface waves of the type detected on the deep sea floor must also exist along the shore. They are difficult to observe, however, because of very energetic processes in the adjacent bands, tides on one side, normal wind waves on the other, and also because of complicated interactions along the shore line involving local circulation and wind, such as edge waves, wind set-up, shoaling transformation, surf beat, etc. For this reason the actual character of the very-low-

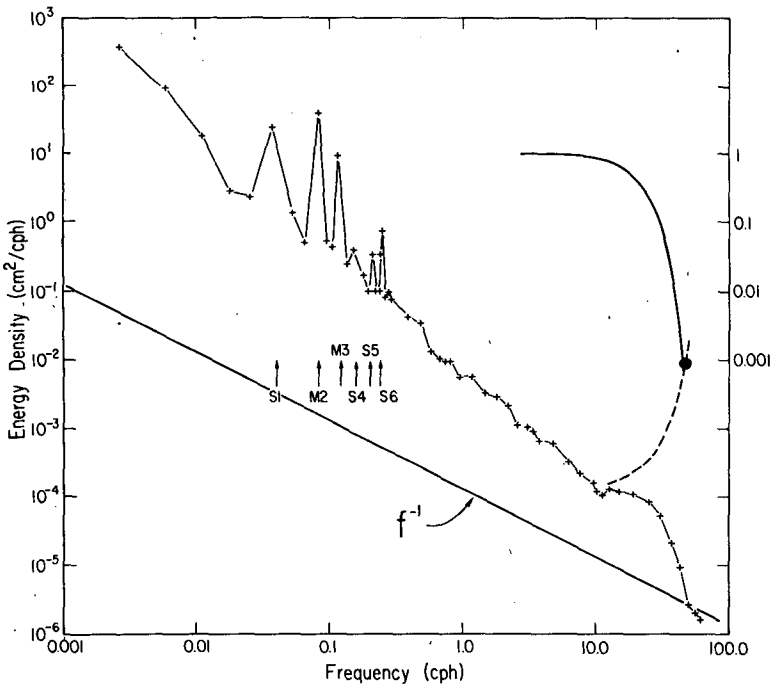

FIG. 6. Complete power spectrum of residual fluctuations up to the Nyquist frequency of 64 cph. The pressure response of ordinary gravity surface waves on the sea floor (for a local depth of 5.7 km) is indicated above (dark line) and the implied surface-wave spectrum is shown by the dashed line. The single, dark point corresponds to 100 s waves in 30 m depth at Camp Pendleton, California. The large peaks at diurnal, semidiurnal and higher harmonics are the tidal cusps discussed in the text.

frequency end of the wind-wave spectrum ($T > 1$ min), even along the shore, is still much in doubt. We have nevertheless plotted in Fig. 6 one of the very rare coastal estimates available, namely the average energy density of sea-surface fluctuations with a period of 100 s at Camp Pendleton, California (Munk, 1962), although the author warns of day-to-day deviations of the order of one decade, up or down. The match between this value and our open-ocean observations is embarrassing by its perfection, considering the large uncertainties in both.

In spite of the plausibility of the previous interpretation of deep sea-floor pressure fluctuations with several-minute periods as manifestations of ordinary surface waves, another mechanism may contribute to these same fluctuations. Larsen (1978) suggests that wave packets may force long gravity waves capable of penetration to the very bottom in deep water. While it appears unlikely that the surprisingly high observed amplitudes could be generated by this process, a definite answer could be readily obtained by means of an appropriate sea-floor array. Directional spectra would provide information on propagation velocities and coherence scales. It is also conceivable that part of the low-frequency wave-interaction energy near sea shores, for instance in surf beat (Munk, 1949), radiates offshore.

Except for the features discussed earlier—diurnal, semidiurnal and higher tidal harmonic cusps, and low-frequency wind waves—the energy spectrum of the residual pressure fluctuations on the sea floor is relatively smooth (see Fig. 6). Apart from the various peaks already explained, its trend remains relatively linear in a log-log space over at least three frequency decades with a slope of about -1.6.

The clear identification of the surface-wave spectral feature indicates its definite resolution above noise. The sudden interruption of its abrupt high-frequency cutoff is a good indication that the high-frequency noise level is not higher than that represented by the last points to the extreme right of the energy spectrum of Fig. 6. At frequencies below a few cycles per second the noise-energy level in instrumentation relying on electronic amplification is generally characterized by a f^{-1} dependence. If one tentatively assumes that the background noise characterizing the very long-term instrumental stability has this f^{-1} dependence then all fluctuations shown on Fig. 6 must be real. If so, what processes are involved? Again, an adequate instrumental array would be invaluable in investigating this question.

Although one may be tempted to rule out internal waves on the basis of the absence of a conspicuous high-frequency cutoff in the neighborhood of 2–5 cph (Garrett and Munk, 1975), we shall see later that such a cutoff is often observed. Other possible candidates include bottom turbulence, response to irregularity in wind stress, and atmospheric pressure variability.

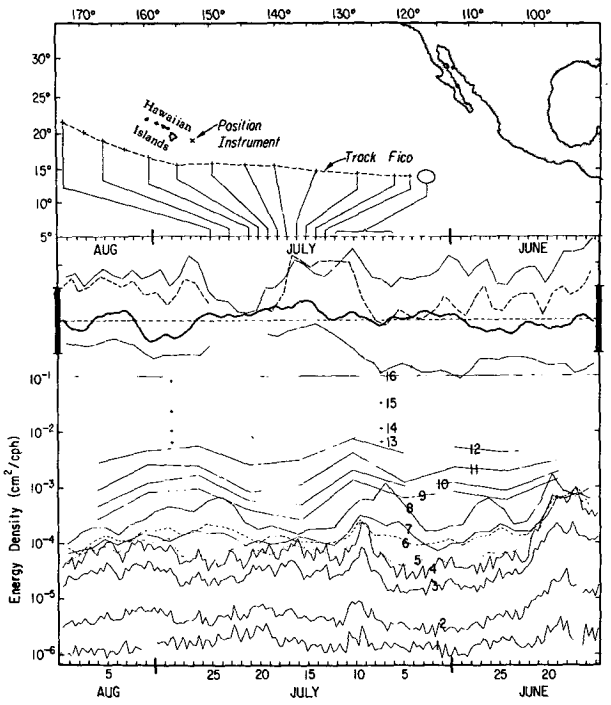

FIG. 7. The upper box represents on a map of the northeast Pacific the track of Tropical Cyclone Fico. In the central box the heavy line corresponds to the long-term fluctuations as shown on the lower curve of Fig. 1. Here, however, the time has been made to run from right to left, as does the track of Fico. The upper fine line is the atmospheric pressure at Hilo and the lower one is the sea level at Hilo. The dashed line represents the equivalent pressure on the bottom at Hilo (sea level plus atmospheric pressure). The resolution is 5 times greater for the deep-sea-floor pressure: the dark bars at left and right correspond to 10 cm for the deep-sea-floor pressure, 50 cm and 50 mb for the other three. On the lower box are shown the running energy spectra of high-frequency fluctuations in the residual pressure record. Frequency-band center and band width are indicated in Table 4 for 16 bands.

7. Signature from Tropical Cyclone Fico

During the experiment, Tropical Cyclone Fico formed off the coast of Mexico around 14°N, 118°W and traveled westward to the south of the pressure-recorder location with a closest approach of about 350 km on 20 July 1978. We wondered whether some distinct signature would occur in the pressure signal at its passage. While the results are in a sense disappointing, the special presentation of the data arranged on Fig. 7 to facilitate this investigation permits a practical examination of the ensemble of the sea-floor pressure fluctuations for the duration of the record.

TABLE 4. Band numbers, center frequencies and band widths for running power spectra of residual fluctuations.

Band number	Center frequency (cph)	Band width (cph)
1	58	12
2	46	12
3	34	12
4	22	12
5	14.8	3
6	11.8	3
7	8.8	3
8	5.8	3
9	3.6	0.75
10	2.9	0.75
11	2.1	0.75
12	1.4	0.75
13	0.9	0.2
14	0.7	0.2
15	0.5	0.2
16	0.35	0.2

A map of the southeastern quadrant of the North Pacific Ocean is reproduced at the upper part of Fig. 7, indicating the position of the pressure recorder (18°56'N, 152°29'W) and the track of Fico. Just below, in the central part of the figure, four curves represent, respectively, the smoothed sea-floor pressure fluctuations (dark line), the atmospheric pressure at the closest possible station (Hilo), 330 km due west (fine continuous upper line), the smoothed sea level at Hilo (fine continuous lower line) and the sum of sea level and atmospheric pressure at Hilo (dashed line). The last three curves are plotted at a scale one-fifth that of sea-floor fluctuations for convenience. In order to make the correspondence between the position of Fico, moving westward, and possible synchronous features of the records more obvious, the time is running from right to left. In the lower part, the running spectral energy levels of high-frequency signals are plotted similarly. The center frequencies and bandwidths of the various bands, numbered 1 to 16, are listed in Table 4.

With respect to the very low-frequency signals represented on the central part of Fig. 7, no significant correlation can be noticed except the very large drop in atmospheric pressure with its low point corresponding to the closest approach. Most significant, therefore, is the absence in the sea-floor pressure of any counterpart to the very low atmospheric pressure that persisted for over a week, an indication that the inverted barometer compensation was virtually complete.

The absence of visual correlation between bottom pressure at the deep-sea site and at Hilo (sea level plus atmospheric pressure) is surprising and it is contrary to the results of similar comparisons in the MODE area (Brown *et al.*, 1975). The disabling of the Hilo bubbler tide gage during the storm, however, weakens this conclusion.

In the lower part of Fig. 7 the energy levels in the bands 1–6 correspond to the postulated surface wave contributions. Their variability with time is substantial (at least one decade). The changes are gradual and significant over time spans larger than a day or two. The high-frequency cut-off is frequency-independent and always abrupt. We have tried to correlate the changes in this band with meteorological patterns: weather maps indicate that the most energetic period, 14–22 June, corresponds to unusually strong trade winds blowing over an extended fetch of the Northeast Pacific. In our correlation attempt we have been handicapped by the impossibility of deriving propagation direction in the absence of an array of stations. We have not been able either to use dispersion properties in the manner described by Munk (1947b) and Snodgrass *et al.* (1966) to infer the distance to the source because the waves involved are nearly non-dispersive. Their wavelength is several times the water depth and they travel at, or very nearly at, the shallow water-wave velocity $(gh)^{1/2}$ (g acceleration of gravity, h ocean depth). In spite of the observed spectral variability in this low frequency portion of the wind-wave band, no spectacular signature can be conclusively ascribed to Fico. One feature of interest is present, nevertheless, namely, a temporary rise of activity around 6 July, lasting several days and simultaneous with the formation and stationary phase of Fico. Again we have no way to relate this event to the generation by Fico of very long wave forerunners (Munk, 1947a) in the absence of information on propagation.

If the high-frequency internal-wave cutoff observed in oceanographic data (Garrett and Munk, 1975) has a detectable signature in the sea-floor pressure, this effect would probably affect band 8, which covers the range 4.4 to 7.3 cph, or possibly band 9. A spectral valley then would be expected between the low-frequency surface-wave cutoff and the high-frequency internal-wave cutoff. This would mean that the spacing between traces 8 and 7 (Fig. 7) should be significantly larger than between the neighboring bands, a situation often, though not always, true. (The small inflection around 10 cph on Fig. 6 involves significantly only the low-frequency surface-wave cutoff).

8. Very long-term fluctuations

Recent progress in our understanding of large scale air-sea interactions suggests the possibility of great advances in long-term forecasting in the forseeable future (Barnett, 1980). A variety of puzzling correlations between climatic events widely separated in space and time has been documented. For

instance, dramatic changes in coastal meteorology and oceanic circulation, such as El Niño along the coast of Peru, have been shown to be preceeded by distinct changes in sea level and other oceanographic parameters in distant oceanic areas (Wyrtki, 1974, 1975; Hickey, 1975). There is at least very suggestive evidence in the relevant literature that the dynamics associated with some of these processes involves baroclinic waves more or less trapped within the tropics (Wunsch and Gill, 1976; Moore and Philander, 1976). Although very small, the pressure signature on the deep-sea floor of the first two or three baroclinic modes of several of these propagating features should be well above the overall energy level (instrumental plus background) characteristic of the data presently discussed. In particular, the pressure signals from the higher modes of equatorially-trapped Kelvin waves capable of transferring a significant portion of the energy believed to travel eastward in equatorial oceans would have to be so large that, if existing, they must be readily detectable. Since their velocity field is entirely zonal, vertical electric-field recorders (Harvey, 1974) that record this component selectively and with precision could be associated with pressure recorders in an equatorial array to establish or to refute the existence of such waves.

More recently it has been suggested that large-scale features of oceanic circulation associated with eastward-traveling cyclonic perturbations at moderate-to-high latitudes must penetrate to the sea floor, their associated pressure signals suffering only limited attenuation (Philander, 1978). If this is so, the simplicity, modest cost and very long endurance of sea-floor pressure recorders deployed in appropriate arrays could contribute data well suited to a study of the mechanisms involved in the mechanical coupling of the oceanic circulation to its atmospheric driving. In this respect, the dominant feature among the very-long-term fluctuations that occur around 26 July and last about one week, with a maximum pressure excursion around 4 cm equivalent water head, could be the remnant of a deep, relatively large-scale perturbation of the central tropical Pacific circulation initially generated by Fico (Fig. 7).

The results discussed here can help assess the value of undertaking investigation of certain large-scale, long-term features of oceanic circulation and ocean-atmosphere interactions by including information on ocean-floor pressure signals to more classic types of data. For this purpose the present evidence is limited by the two-month duration of the observations. As visible on Fig. 5, the frequency band of interest, roughly the band below 0.03 cph ($T > 1\frac{1}{2}$ day), is represented by only about 40 Fourier lines. As expected from natural statistical fluctuations, a few of these lines conspicuously exceed the local average. If they are taken as indicators of the maximum encounterable competing background noise level, the following values are of interest: 0.7 cm aplitude at 9-day periodicity, 0.3 cm at 3.7 day, 0.1 cm at 2.1 day, 0.1 cm at 38 hour (bandwidth 7.3×10^{-4} cph).

Another clue of interest is the degree to which the lunar fortnightly tide is resolved. The amplitude and phase of constituent *Mf* derived from the tide analysis (see Table 2) are 0.84 cm and $-15°$, with 0.91 cm for the equilibrium tide, leading to an admittance modulus of 0.93. The latter should be smaller, probably close to 0.7 (Melchior, 1966), to take into account the solid earth response to gravitational and loading forces and the phase should be small, as observed, but with the opposite sign. Taken together these considerations lead to a maximum error of 0.3 cm. This favorable result may be largely fortuitous; it may also be due to an inherently reduced oceanic noise in that band, far offshore.

9. Conclusion

We hope that this paper will contribute to the acceptance of the legitimacy of drift removal in Bourdon-tube-type sea-floor pressure transducers by means of the techniques described earlier. We believe that for the time being this acceptance will prove more beneficial than efforts restricted to a search for nothing less than a truly absolute pressure transducer, which might only confirm the elusiveness of this objective. We want to emphasize, of course, that the correction afforded by the proposed approach is not a complete correction by any means. There is no criterion, for instance, that permits one to know or even guess from the recorded data the pressure difference between the beginning and the end of the record; only an upper limit presently considerably larger than any conceivable real occurrence can be estimated. It is also difficult to prevent the drift-optimizing scheme from acting upon real long-term curvature with periods longer than the record length. For periods shorter than the record this effect falls abruptly with the harmonic number. This is so because the plastic flow curvature decreases very rapidly with time and most of the error results overwhelmingly from the mismatch at the very beginning between assumed and true creep. In trying to visualize the meaning of this dedrifting technique it is essential to bear in mind that it is not a filtering technique. It relies, on the contrary, upon deterministic rather than statistical information with considerable weight in constraining the drift function.

The situation is in fact more favorable than immediately apparent for other reasons. Because the optimum shape of the Bourdon tube cross-section

is not simple to produce, we have begun our research using fully annealed stock material much easier to form but much less subject to benefit from age-hardening heat treatment. Furthermore, plastic flow is a very nonlinear and rapidly increasing function of stress. The latter can be reduced by increasing the sensitivity of the optical detector, an option nearly, yet not fully exhausted. Thus the drift level may still likely be reduced by a factor of 10, perhaps by a factor of 100 or more. Since plastic strain rate decreases with time, the long-term performances of the instrumentation should improve with the duration of observations.

The experiment described here is the first step in a series of field operations of a broader nature with the twin purpose of optimizing a promising sea-floor pressure transducer for sensitive, long-term observations, and of collecting important oceanographic data that do not require, as yet, exhaustive performances from the transducer. Open-ocean tides constitute prime targets for this initial purpose, and, since the field experiments can be carried out in conjunction with a compatible program of sea-floor magnetotellurics that takes us far from coasts or islands where tidal response is not directly known, our multipurpose approach can be productive while still remaining economical. It is even justifiable in the sense that the remarkable temperature stability on the sea floor and the precise knowledge of pressure could be duplicated in the laboratory only at extremely high costs. Thus, even independently from the by-product of geophysical data acquisition, experimentation on the deep-sea floor may be advantageous for research and development purposes alone.

A limitation of the geophysical results presented here is a consequence of observations restricted to a single site. An instrumental array would greatly contribute to the understanding of features not clearly identifiable by revealing their propagation direction and velocity as well as their coherence scales. Nevertheless, the quantitative conclusions related to tides, the surprising resolution of constituent Mf, and the postulated detection of the low-frequency end of the surface wind-wave spectrum are indicators of the potential data returns from sea floor observations over appropriate arrays.

Acknowledgments. Critical comments and many constructive suggestions from K. E. Kenyon are greatly appreciated. Hawaiian tide data were kindly made available to us by J. E. Fancher and D. L. Porter. This work has been supported by the National Science Foundation, Grants OCE 77-20625 and OCE 78-25324.

REFERENCES

Andrade, E. N., 1910: On the viscous flow in metals and allied phenomena. *Proc. Roy. Soc., London*, **A84**, 11.

Baker, D. J., and R. B. Wearn, 1973: Pressure and temperature measurements at the bottom of the Sargasso Sea. *Proc. Nat. Phys. Soc.*, **245**, 25–26.

Barnett, T. P., 1981: Statistical predictions of North American air temperature from Pacific predictors. *Mon. Wea. Rev.* (in press).

Brown, W., W. Munk, F. Snodgrass, H. Mofjeld and B. Zetler, 1975: MODE bottom experiment. *J. Phys. Oceanogr.*, **5**, 75–85.

Caldwell, D. R., F. Snodgrass and M. Wimbush, 1969: Sensors in the deep sea. *Phys. Today*, 34–42.

Cartwright, D. E., B. D. Zetler and B. V. Hamon, 1979: Pelagic tidal constant. *IAPSO Publ. Sci.*, No. 30.

Eyriés, M., M. Dars and L. Eldely, 1964: Maregraphic par grands fonds. *Cah. Oceanogr.*, **16**, 782–798.

Filloux, J. H., 1969: Bourdon tube deep sea tide gauges. *Tsunami in the Pacific Ocean*, W. M. Sams, Ed., East West Center Press, 223–238.

——, 1970: Deep sea tide gauge with optical readout of Bourdon tube rotation. *Nature*, **226**, 936–938.

——, 1971: Deep sea tide observations from the northeastern Pacific. *Deep-Sea Res.*, **18**, 275–284.

——, 1973: Tidal patterns and energy balance in the Gulf of California. *Nature*, **243**, 217–221.

——, 1980: Observation of very low frequency electromagnetic signals in the ocean. *J. Geomagn. Geoelectr.*, **32** (Suppl. I) SI 1–SI 12.

——, 1981: Magnetotelluric exploration of the North Pacific: Progress Report and preliminary soundings near a spreading ridge. *Tectonophysics* (in press).

——, and R. L. Snyder, 1979: A study of tides; set up and bottom friction in a shallow semi-enclosed basin. Part I: Field experiment and harmonic analysis. *J. Phys. Oceanogr.*, **9**, 1979.

Frankignoul, C., and P. Müller, 1979: Quasi-geostrophic response of an infinite β-plane ocean to stochastic forcing by the atmosphere. *J. Phys. Oceanogr.*, **9**, 104–125.

Garrett, C., and W. Munk, 1975: Space-time scales of internal waves: A progress report. *J. Geophys. Res.*, **80**, 291–297.

Harvey, R. R., 1974: Derivation of oceanic water motions from measurements of vertical electric field. *J. Geophys. Res.*, **79**, 4512–4516.

Hasselmann, K., 1963: A statistical analysis of the summation of microseism. *Rev. Geophys.*, **1**, 177–210.

Haubrich, R. A., W. H. Munk and F. E. Snodgrass, 1963: Comparative spectra of microseisms and swell. *Bull. Seismol. Soc. Amer.*, **53**, 27–37.

Hayes, S. P., 1979: Variability of current and bottom pressure across the continental shelf in the northeast Gulf of Alaska. *J. Phys. Oceanogr.*, **9**, 88–103.

Hendershott, M. C., 1973: Ocean tides. *Trans. Amer. Geophys. Union*, **54**, 76–86.

Hickey, B., 1975: The relationship between fluctuations in sea level, wind stress, and sea surface temperature in the equatorial Pacific. *J. Phys. Oceanogr.*, **5**, 460–475.

Hicks, S. D., A. J. Goodheart and C. W. Isely, 1965: Observations of the tides on the Atlantic Continental Shelf. *J. Geophys. Res.*, **70**, 1827–1830.

Irish, J. D., and F. E. Snodgrass, 1972: Quartz crystals as multipurpose oceanographic sensors, I. Pressure. *Deep-Sea Res.*, **19**, 165–169.

Larsen, J. C., 1977: Cotidal charts for the Pacific Ocean near Hawaii using f-plane solutions. *J. Phys. Oceanogr.*, **7**, 100–109.

Larsen, L. H., 1978: The effect of finite depth on the propagation of nonlinear wave packets. *J. Phys. Oceanogr.*, **8**, 923–925.

Latham, G., R. Anderson and M. Ewing, 1967: Pressure variations produced at the ocean bottom by hurricanes. *J. Geophys. Res.*, **72**, 5693–5704.

Longuet-Higgins, M., 1950: A theory of the origin of microseisms. *Phil. Trans. Roy. Soc. London*, **A243**, 1–35.

Melchior, P., 1966: *The Earth Tides*. Pergamon Press, 26–38.

Moore, D. W., and S. G. H. Philander, 1976: Modeling of the tropical ocean circulation. *The Sea*, Vol. 6, E. D. Goldberg *et al.*, Eds., Wiley (see pp. 319–361).

Mott, N. F., 1953: A theory of work hardening of metal. Flow without slip lines, recovery and creep. *Phil. Mag.*, **44**, 742–765.

Munk, W. H., 1947a: Tracking storms by forerunners of swells. *J. Meteor.*, **4**, 45–57.

——, 1947b: Increase in the period of waves traveling over large distances with application to tsunami, swell and seismic surface waves. *Trans. Amer. Geophys. Union*, **28**, 198–217.

——, 1949: Surf beats. *Trans. Amer. Geophys. Union*, **30**, 849–854.

——, 1962: Long ocean waves. *The Sea*, Vol. 1, M. N. Hill, Ed., Wiley, pp. 647–663.

——, and D. E. Cartwright, 1966: Tidal spectroscopy and prediction. *Phil. Trans. Roy. Soc. London*, **A259**, 564–581.

——, F. Snodgrass and M. Wimbush, 1970: Tides off-shore: Transition from California coastal to deep sea waters. *Geophys. Fluid Dyn.*, **1**, 161–235.

——, and B. D. Zetler, 1967: Deep sea tides: a program. *Science*, **158**, 884–886.

Neumann, G., and W. J. Pierson, Jr., 1966: The astronomical tides of the oceans. *Principles of Physical Oceanography*, Prentice Hall, 298–310.

Nowroozi, A. A., G. H. Sutton and B. Auld, 1966: Oceanic tides recorded on the sea floor. *Ann. Geophys.*, **22**, 512–517.

Oliver, J., and J. Dorman, 1961: On the nature of oceanic seismic surface waves with prominent periods of 6–8 seconds. *Bull. Seismol. Soc. Amer.*, **51**, 437–455.

Philander, S. G. H., 1978: Forced oceanic waves. *Rev. Geophys. Space Phys.*, **16**, 15–46.

Radok, R., W. Munk and J. Isaacs, 1967: A note on mid-ocean internal tides. *Deep-Sea Res.*, **14**, 121–124.

Schwiderski, W. W., 1980: On charting global ocean tides. *Rev. Geophys. Space Phys.*, **18**, 243–268.

Snodgrass, F. E., 1968: Deep sea instrument capsule. *Science*, **162**, 78–87.

——, G. W. Groves, K. F. Hasselmann, G. R. Miller, W. H. Munk and W. H. Powers, 1966: Propagation of ocean swell across the Pacific. *Phil. Trans. Roy. Soc. London*, **A1103**, 431–497.

UNESCO, 1975: An intercomparison of open sea tidal pressure sensors. Rep. SCOR Working Group 27, Tides of the Open Sea, *UNESCO Tech. Pap. Mar. Sci.*, **21**, 56–58 pp.

Wunsch, C., and J. Dahlen, 1974: A moored temperature and pressure recorder. *Deep-Sea Res.*, **21**, 145–154.

——, and A. E. Gill, 1976: Observations of equatorially trapped waves in Pacific sea level variations. *Deep-Sea Res.*, **23**, 371–390.

Wyrtki, K., 1974: Sea level and seasonal fluctuations of the equatorial currents in the western Pacific Ocean. *J. Phys. Oceanogr.*, **4**, 91–103.

——, 1975: Fluctuations of the dynamic topography in the Pacific Ocean. *J. Phys. Oceanogr.*, **5**, 450–459.

Zetler, B. D., 1967: Tides and other long period waves. U.S. Nat. Rep., 14th General Assembly, *Trans. Amer. Geophys. Union*, **48**, 591–595.